Molecular Structure and Vibrational Spectra of Iodotrimethylgermane ($GeIMe_3$) by Theory and Experiment

María L. Roldán,[†] Silvia A. Brandán,[†] Sarah L. Masters,[‡,§] Derek A. Wann,[‡] Heather E. Robertson,[‡] David W. H. Rankin,[‡] and Aída Ben Altabef*[,†]

Instituto de Química Física, Facultad de Bioquímica, Química y Farmacia, Universidad Nacional de Tucumán, San Lorenzo 456, 4000 Tucumán, Argentina, and School of Chemistry, University of Edinburgh, West Mains Road, Edinburgh, EH9 3JJ U.K.

Received: March 16, 2007; In Final Form: May 7, 2007

The geometry of iodotrimethylgermane has been determined by experimental and computational methods. Fourier transform infrared spectra have been recorded over a range of temperatures along with the Raman spectrum to obtain comprehensive vibrational data for the fundamental modes. The stretching, rocking, and deformation bands of the methyl groups have been resolved into their components with the aid of low-temperature infrared spectroscopy using Fourier self-deconvolution and curve-fitting methods. The optimized geometries and vibrational harmonic frequencies were calculated by density functional theory methods employing Pople-type basis sets, as well as those with descriptions for an effective core potential describing both germanium and iodine atoms. A scaled quantum mechanical analysis was carried out to yield the best set of harmonic force constants and obtain a transferable set of scale factors that can be applied to the $(CH_3)_3$-GeX (X = H, Cl, Br, I) series.

Introduction

The first preparation of iodotrimethylgermane (ITMG) was reported in 1954,[1] with a report of direct synthesis in 1964.[2] Since then, very little work has been performed with ITMG, and no structural work in the form of gas-phase or solid-phase diffraction or rotational spectroscopy has ever been reported. ITMG has uses as a germanium promoter in the preparation of propylene glycol monoalkyl ethers and alkoxyacetones.[3]

In this paper, we report the molecular structure of ITMG and an improved vibrational assignment. By combining gas-phase electron diffraction and ab initio methods, we have been able to obtain a reliable structure, especially for parameters relating to iodine, which are notoriously difficult to calculate precisely.

The only previous work related to the study of the vibrational spectra of ITMG was performed by Anderson et al.[4] as part of the vibrational analyses of halogenated derivatives of $(CH_3)_nGeI_{4-n}$ ($n = 1, 2, 3$). IR spectra were recorded in the gas and liquid phases, while Raman spectra were obtained in the liquid phase. Most of the expected vibrational modes were assigned for the molecule. However, they observed broad bands for the CH_3 stretching, the CH_3 rocking, and the CH_3 deformation normal modes in the vibrational spectra, and these modes could not be assigned individually.

The main aim of the work reported in this paper is to complete the assignments of these fundamental modes by using quantum mechanical calculations, data provided from low-temperature IR spectroscopy, and the techniques of Fourier self-deconvolution and curve-fitting. In addition, a natural bond orbital analysis of the molecular wave function ψ was performed. In order to find useful extensions of bonding concepts of Lewis structure in this type of compound, the analysis was applied to both $(CH_3)_3GeI$ and $(CH_3)_3SiI$ compounds.

Experimental Section

Raman and Infrared Spectroscopy. Iodotrimethylgermane was obtained from ABCR (98% purity) and used without any further purification, avoiding light exposure and atmospheric humidity. The Fourier transform infrared (FTIR) spectra of the sample were recorded at room and low temperatures in the range 4000−400 cm^{-1} on a Perkin-Elmer Model GX FTIR spectrophotometer, with a resolution of 2 cm^{-1} and 64 scans. The room-temperature infrared (RTIR) spectrum was recorded as a film between KBr windows. Low-temperature infrared (LTIR) spectra of the liquid were measured at different temperatures, using liquid nitrogen to cool the samples. These spectra were run in a variable-temperature RIIC (VLT-2) cell equipped with AgCl windows. The Raman spectrum of the liquid was recorded with a FT-Raman Bruker RFS 100 spectrophotometer, equipped with a Nd:YAG laser (excitation line 1064 nm) and a liquid N_2 cooled Ge detector. The spectrum of the sample was recorded with a resolution of 1 cm^{-1} and 200 scans. The measurement of the parallel and perpendicular polarized Raman spectra determined the depolarization ratios, which describe the symmetry properties of normal vibrations.

The RTIR spectrum is shown in Figure 1 and the overlaid parallel and perpendicular Raman spectra are shown in Figure 2. The observed vibrational frequencies in the infrared and Raman spectra and the assignments of the vibrational normal modes of the molecule are shown in Table 1. All the remaining observed bands that are not assigned to fundamental modes in the infrared and Raman spectra have been assigned to combination bands and overtones. Only one combination is suggested for each band, although several possibilities arise for some of

* Corresponding author. Telephone: +54 381 4311044. Fax: +54 381 4248169. E-mail: altabef@fbqf.unt.edu.ar.
[†] Universidad Nacional de Tucumán.
[‡] University of Edinburgh.
[§] Née Hinchley.

10.1021/jp072111r CCC: $37.00
Published on Web 07/12/2007

TABLE 1: Observed Bands in the Infrared and Raman Spectra of ITMG

infrared[a]		Raman				
				assignment[e]		
room temp	low temp[b]	observed[c]	depolarization ratio[d]			
2992 m	2992 w	2991 sh		ν_{13}	ν_a CH_3	E
2981	2981	2979 (14)	0.72 dp	ν_1	ν_a CH_3	A_1
2975	2975			ν_{14}	ν_a CH_3	E
2910 sh	2910 w	2908 (80)	0.15 p	ν_2	ν_s CH_3	A_1
2906 m	2905			ν_{15}	ν_s CH_3	E
	1418	1414[f] sh		ν_3	δ_a CH_3	A_1
1405 m	1407 m	1405[f] (2)	0.75 dp	ν_{16}	δ_a CH_3	E
	1399	1397[f] sh		ν_{17}	δ_a CH_3	E
1240 s	1244 s	1249[f] (7)	0.23 p	ν_4	δ_s CH_3	A_1
	1232	1235[f] sh		ν_{18}	δ_s CH_3	E
829 s	845 vs	843[f] sh		ν_{19}	ρ CH_3	E
	826	833[f] (1)	0.17 p	ν_5	ρ CH_3	A_1
763 m	763 m	760 (0.6)	0.66 dp	ν_{20}	ρ CH_3	E
614 s	617 vs	614 (12)	0.65 dp	ν_{21}	ν_a GeC_3	E
568 s	568 s	569 (100)	0.11 p	ν_6	ν_s GeC_3	A_1
		220 (46)	0.16 p	ν_7	ν GeI	A_1
		189[f] sh	0.75[g] dp	ν_{22}	δ_a GeC_3	E
		176[f] (35)	0.47 p	ν_8	δ_s GeC_3	A_1
		142 (17)	0.66 dp	ν_{23}	ρ GeC_3	E
		112 (4)	0.44 dp	ν_{24}	τ CH_3	E

[a] w, weak; m, medium; s, strong; vs, very strong; sh, shoulder. [b] From the infrared spectrum of a sample cooled in liquid nitrogen. [c] Relative intensity in parentheses. [d] p, polarized; dp, depolarized. [e] ν, stretching; δ, angular deformation; ρ, rocking; τ, torsion; s, symmetric; a, antisymmetric. [f] From Fourier self-deconvolution. [g] From curve-fitting.

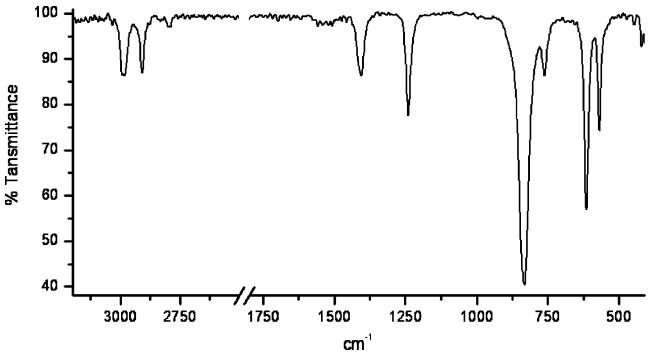

Figure 1. FTIR spectrum of ITMG at room temperature.

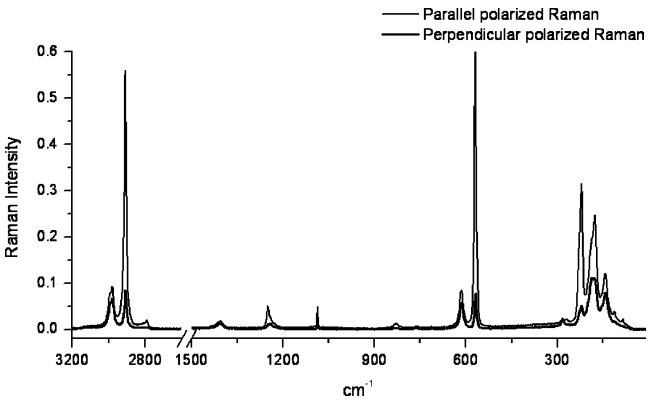

Figure 2. Parallel and perpendicular polarized Raman spectra of ITMG.

them. The frequencies of these bands and their assignments are shown in Table 2.

Spectral Analysis. Curve-fitting and Fourier self-deconvolution were performed using the standard software of the infrared spectrophotometer.[5] Fourier self-deconvolution (FSD) and curve-fitting are two of the many numerical methods for the analysis of infrared and Raman spectra that provide reduction of spectral bandwidth and resolution enhancement. FSD estimates the number and position of the band components, while curve-fitting provides information about intensities. The FSD technique is

TABLE 2: Assignment of Combination Bands and Overtones Observed in the Vibrational Spectra of ITMG

IR	Raman	assignment	
3825		$\nu_1 + \nu_{19}$	(=3821)
3744		$\nu_1 + \nu_{20}$	(=3740)
3662		$\nu_{15} + \nu_{20}$	(=3669)
3177		$\nu_{13} + \nu_{22}$	(=3179)
3112	3109	$2\nu_4 + \nu_{21}$	(=3112)
2805	2804	$\nu_1 - \nu_8$	(=2803)
2792	2791	$\nu_1 - \nu_{22}$	(=2790)
2461	2463	$2\nu_{21} + \nu_{18}$	(=2463)
2082		$\nu_4 + \nu_{19}$	(=2082)
	1929	$2\nu_4 - \nu_6$	(=1929)
1855		$\nu_4 + \nu_{21}$	(=1854)
1805		$\nu_4 + \nu_6$	(=1808)
1520		$2\nu_{20}$	(=1520)
	1086	$2\nu_{21} - \nu_{23}$	(=1086)
	713	$\nu_6 + \nu_{23}$	(=711)
	702	$\nu_{19} - \nu_{23}$	(=701)
680		$\nu_6 + \nu_{24}$	(=680)
670		$\nu_4 - \nu_6$	(=672)
657		$\nu_5 - \nu_8$	(=654)
452		$\nu_6 - \nu_{24}$	(=456)
	282	$2\nu_{23}$	(=284)
	268	$2\nu_{22} - \nu_{24}$	(=266)
	84	$\nu_{13} - \nu_2$; $\nu_{19} - \nu_{20}$	(=83)

based on the method described by Kauppinen et al.[6−8] The selected region of the spectrum is inverse Fourier transformed to yield an interferogram. The inteferogram is then treated with a Bessel apodization function and two enhancement factors *W* and *K* to produce narrower band shapes. *W* is defined as the bandwidth at half-height, and *K* is the enhancement parameter defined as the ratio of bandwidths of the original and enhanced bands. After this procedure the resulting interferogram is transformed back to the frequency domain. The curve-fitting method was originally established by Griffiths et al.[9] and is based on the least-squares optimization of all the band parameters, namely intensity, frequency, half-bandwidth, and band shape.

The analysis of the Raman spectra involves the combination of two methods in a three-step approach previously employed

by other authors.[10,11] First, the bands of the experimental Raman spectrum were deconvoluted after baseline correction, to increase the resolution of the bands and to provide their estimated positions. Following FSD, the spectrum was curve-fitted to obtain the accurate number and positions of its components. The baseline-corrected experimental spectrum was then also fitted using the frequency positions and band shape determined in the previous step. The intensity and bandwidth parameters were optimized during the calculations. Consistency between the deconvoluted fitted spectrum and deconvoluted experimental spectrum can then be used as an essential criterion for accepting the curve-fitting parameters and verifying the existence of the bands.

Gaussian peak shapes were used in the curve-fitting routine. The output of the calculations provides a value for the standard deviation, which is the sum of the squares of the residuals between the data and the best-fit curve. The deviations on the measured spectra for the calculations were below 0.1 cm^{-1}.

Computational Methods. The structure of the molecule was investigated using C_{3v} symmetry. An experimental gas-phase investigation of the related iodotrimethylsilane revealed that allowing the structure the freedom to deviate from C_{3v} to C_3 symmetry caused no change to the structure.[12] Therefore, the related iodotrimethylgermane was modeled with C_{3v} symmetry only. Calculations were performed using the Gaussian 03 program.[13]

A series of calculations combining the hybrid functional B3LYP or MP2 methods with the 6-311G, 6-311G*, 6-311G**, LanL2DZ effective core potential (ECP), or LanL2DZdp basis sets were used to calculate the vibrational frequencies and infrared intensities. These calculations determined the best theoretical approximation to predict the vibrational frequencies, and parameters obtained with them are given in Table S1 (Supporting Information).

The method and the basis set that gave the best fit to the observed experimental frequencies were used to calculate the harmonic force field. This force field was transformed from Cartesian coordinates to symmetry coordinates and then scaled according to Pulay's scheme.[14−16] This methodology involves multiplying the main force constants by the scale factor f_i and the corresponding interaction constants by $(f_i, f_j)^{1/2}$, adjusting them to reproduce the experimental frequencies as accurately as possible.

Estimates of the amplitudes of vibration (u) for use in the gas electron diffraction (GED) refinement were also required. The analytic second derivatives of the energy with respect to the nuclear coordinates calculated at the MP2 level with the LanL2DZ basis set gave force fields, which were used to provide these estimates.

The potential-energy distribution (PED) was calculated with the resulting scaled quantum mechanical force field (SQMFF), in which the relative contribution of each symmetry coordinate to the normal modes of vibration is represented. The SQM force field was also used to calculate the force constants, expressed as simple valence internal coordinates.

The conversion of the force constants, fitting of the scale factors, and potential-energy distribution calculation were performed using the program FCARTP.[17] The natural bond orbital calculation was performed using the NBO 3.0 program,[18] as implemented in the Gaussian 03 package with the 6-311G** and LanL2DZdp basis sets, on the previously fully optimized molecular geometry.

After the GED investigation was complete, a discrepancy between the experimental [254.4(1) pm] and theoretical (260.2 pm; B3LYP/6-311G**) Ge−I bond lengths was observed. An MP2 calculation with the correlation consistent basis set aug-cc-pVTZ was performed, with the SDB-aug-cc-PVTZ variant (with an ECP) used for Ge and I.

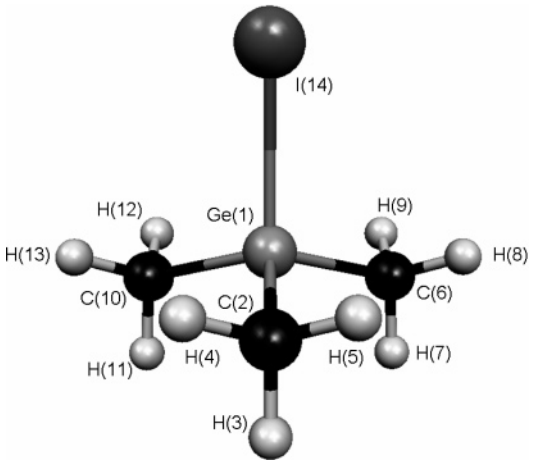

Figure 3. Molecular geometry of ITMG showing atom labeling.

Gas Electron Diffraction. Data were collected for ITMG using the Edinburgh gas-phase electron diffraction apparatus.[19] An accelerating voltage of around 40 kV was used, representing an electron wavelength of approximately 6.0 pm. Scattering intensities were recorded on Kodak Electron Image films at nozzle-to-film distances of 285.68 and 128.16 mm, with sample and nozzle temperatures held at 293 K. The weighting points for the off-diagonal weight matrices, correlation parameters, and scale factors for both camera distances for $GeIMe_3$ are given in Table S2. Also included are the electron wavelengths, as determined from the scattering patterns for benzene, which were recorded immediately after the patterns for the sample compounds. The scattering intensities were measured using an Epson Expression 1680 Pro flatbed scanner and converted to mean optical densities as a function of the scattering variable, s, using an established program.[20] The data reduction and the least-squares refinement processes were carried out using the ed@ed program[21] employing the scattering factors of Ross et al.[22]

Results and Discussion

Theoretical Calculations. The molecular structure of ITMG was investigated with a wide range of ab initio and density functional theory (DFT) methods and an assortment of basis sets. All calculations agreed that the molecule possesses C_{3v} symmetry, with most bond lengths and angles not varying by much. However, the Ge−I distance varied from 260.6 pm (B3LYP/6-311G**) to 263.3 pm (MP2/LanL2DZ), indicating that this parameter may not be well-defined by computational methods. Therefore, comparison with experimental results is needed, as this parameter should be distinct in the radial-distribution curve obtained from the gas electron diffraction experiment.

Gas Electron Diffraction. On the basis of the ab initio calculations described above, electron diffraction refinements were carried out using a model with overall C_{3v} symmetry to describe the gaseous structure, shown in Figure 3 with the atom numbering. The structure was defined in terms of six independent parameters, comprising three bond lengths, two bond angles, and a tilt of the methyl groups. The bond lengths were r(C−H) (p_1), r(Ge−C) (p_2), and r(Ge−I) (p_3). A single C−H bond length was used because the individual ab initio values differed by no more than 0.2 pm. The model also required two

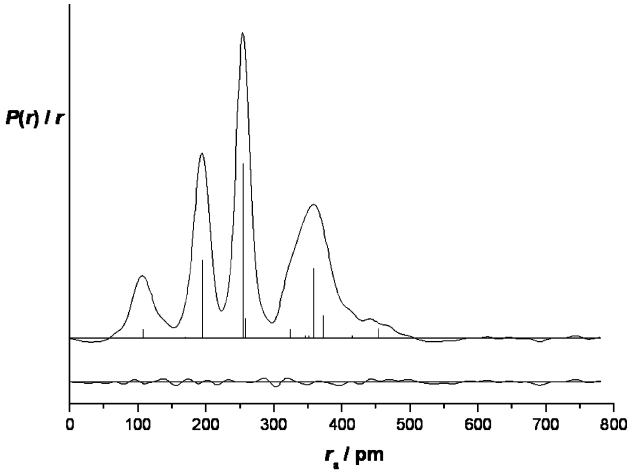

Figure 4. Experimental and difference (experimental − theoretical) radial-distribution curves, $P(r)/r$, for ITMG. Before Fourier inversion the data were multiplied by $s.\exp(-0.00002s^2)/(Z_{Ge} - f_{Ge})(Z_I - f_I)$.

angle parameters, ∠(Ge−C−H) (p_4) and ∠(I−Ge−C) (p_5), providing local C_{3v} symmetry for the methyl groups. The methyl tilt parameter was also included, and a positive tilt indicated a decrease of the unique ∠(Ge−C−H) and an increase of the pair of symmetry-related ∠(Ge−C−H), i.e., away from the Ge−I bond. The starting parameters for the r_{h1} refinement[23] were taken from the theoretical geometry optimized at the MP2/LanL2DZ level. A theoretical (MP2/LanL2DZ) Cartesian force field was obtained and converted into a force field described by a set of symmetry coordinates using the program SHRINK.[23] From this, the root-mean-square (rms) amplitudes of vibration (u_{h1}) and the perpendicular distance corrections (k_{h1}) were generated at the harmonic first-order curvilinear motion approximation. All geometric parameters and six groups of amplitudes of vibration were then refined using the SARACEN method,[24] with flexible restraints employed for three amplitudes of vibration.

The final refinement for ITMG provided a satisfactory fit to the data, with $R_G = 0.079$ ($R_D = 0.047$), and can be assessed on the basis of the radial-distribution curve (Figure 4) and the molecular scattering intensity curves (Figure S1). Final refined parameters are listed in Table 3. The interatomic distances and corresponding rms amplitudes of vibration are given in Table S3. The least-squares correlation matrix is given in Table S4, and the coordinates of the final refined structure from the GED investigation are given in Table S5.

One issue highlighted by the earlier ab initio investigation was the very different values returned for the Ge−I bond length by the various high-level calculations. The MP2 calculation with the LanL2DZ basis set on all atoms returned a value of 263.3 pm, while the B3LYP DFT method with the 6-311G** basis set reduced this length to 260.6 pm. The value for this distance is well-defined in the radial-distribution curve, with the large peak observed at ∼255 pm in Figure 4, confirming that the internuclear distance between the two atoms giving rise to that peak should be well determined. From Table 3, it can be seen that the experimental (r_{h1}) Ge−I distance was 254.4(1) pm. The anharmonic correction to the experimental value was 0.7 pm, giving an r_e value of 253.7 pm for the Ge−I distance. The anharmonic correction (r_{h1} to r_e) was calculated from $3au^2/2$ (where a is taken to be 1.4 from the SHRINK evaluation[23] and u is the rms amplitude of vibration). This equilibrium distance can then be directly compared with the calculated values. An MP2 calculation with the aug-cc-PVTZ basis set on C and H, and the SDB-aug-cc-PVTZ pseudopotential basis set on Ge and I was performed.[25] This returned a Ge−I distance of 255.8 pm, still over 1 pm too long, but much closer than other calculations that had been performed.

The molecular structure of $(CH_3)_3Ge-I$ can be compared to those determined by GED for $(CH_3)_3Ge-X$ (X = Cl or Br).[26] In these cases, C_{3v} symmetry was returned for both molecules, and ab initio calculations agreed that this high level of symmetry was a minimum on the potential energy surface. Ge−C bond lengths (r_g) of 195.0(4) pm (X = Cl) and 195.2(7) pm (X = Br) were observed experimentally, while a Ge−C bond length (r_g) of 194.3(1) pm [r_{h1} = 194.2(1) pm] was observed in this work. Therefore, a slight shortening of the Ge−C bond is observed but no real trend can be established.

There is no crystal structure of ITMG to compare the gaseous structure to, but the solid-state structure of $MeGeI_3$ is known.[27] In this case the average Ge−I bond length was determined to be 250.0(2) pm, significantly shorter than the gaseous Ge−I bond length of 254.4(1) pm for Me_3GeI. The Ge−C bond length is also shorter at 192.0(20) pm compared to 194.2(1) pm in the gaseous structure with three methyl groups. Parameters from gaseous and solid-state structures are not yet directly comparable due to differences in the techniques used to obtain structural parameters. X-ray diffraction measures regions of electron density, while gas electron diffraction measures the internuclear distances. Therefore, a degree of shortening would be expected in the solid-state structure, although this will be very small for the Ge−I bond. The solid-state structure was determined at 290-(2) K, a temperature similar to that in the experimental study of Me_3GeI; therefore, vibrational effects are unlikely to account for the differences. Probably the best explaination is that the three iodine atoms with increased electronegativity shorten all the bonds in $MeGeI_3$, compared to Me_3GeI with just one iodine atom and three less electronegative carbon atoms.

TABLE 3: Refined and Calculated Geometric Parameters for ITMG (Distances in pm, Angles in deg) from the SARACEN GED Study[a,b]

parameter		MP2/LanL2DZ (r_e)	MP2/GEN[c]	GED (r_{h1})	restraint
		Independent			
p_1	r(C−H)	110.6	108.9	107.5(5)	−
p_2	r(Ge−C)	197.7	195.5	194.2(1)	−
p_3	r(Ge−I)	263.3	255.8	254.4(1)	−
p_4	∠[Ge−C−H(av)]	110.5	109.8	113.7(7)	−
p_5	∠(I−Ge−C)	107.1	106.3	105.5(2)	−
p_6	Me tilt			1.3(25)	−
		Dependent			
dp_1	∠[Ge(1)−C(2)−H(3)]	109.8	109.7	112.4(27)	−
dp_2	∠[Ge(1)−C(2)−H(4)]	110.9	109.9	114.4(13)	−

[a] Figures in parentheses are the estimated standard deviations of the last digits. [b] See Supporting Information for parameter definitions. [c] aug-cc-PVTZ on C and H, SDB-aug-cc-PVTZ on Ge and I.

TABLE 4: Comparison of the Calculated Frequencies (cm^{-1}) at B3LYP with 6-311G and LanL2DZdp Basis Sets with the Fundamentals for ITMG**

			B3LYP				
			6-311G*		LanL2DZdp		
mode			unscaled	scaled[a]	unscaled	scaled[b]	exptl
E	ν_a CH_3	ν_{13}	3135	2994	3131	2992	2992
A_2	ν_a CH_3	ν_9	3134	2992	3130	2991	
A_1	ν_a CH_3	ν_1	3116	2976	3112	2974	2981
E	ν_a CH_3	ν_{14}	3114	2973	3111	2973	2975
A_1	ν_s CH_3	ν_2	3037	2907	3034	2907	2910
E	ν_s CH_3	ν_{15}	3035	2905	3032	2905	2905
A_1	δ_a CH_3	ν_3	1476	1417	1469	1419	1418
E	δ_a CH_3	ν_{16}	1464	1406	1457	1408	1407
E	δ_a CH_3	ν_{17}	1460	1403	1455	1405	1399
A_2	δ_a CH_3	ν_{10}	1451	1393	1446	1397	
A_1	δ_s CH_3	ν_4	1288	1243	1280	1241	1244
E	δ_s CH_3	ν_{18}	1276	1233	1267	1232	1232
E	ρ CH_3	ν_{19}	863	847	845	846	845
A_1	ρ CH_3	ν_5	855	838	838	839	826
E	ρ CH_3	ν_{20}	772	754	752	752	763
A_2	ρ CH_3	ν_{11}	736	716	713	710	
E	ν_a GeC_3	ν_{21}	595	616	597	617	617
A_1	ν_s GeC_3	ν_6	549	569	554	572	568
A_1	ν GeI	ν_7	225	222	224	221	220
E	δ_a GeC_3	ν_{22}	171	183	175	187	189
A_1	δ_s GeC_3	ν_8	162	167	163	168	176
E	ρ GeC_3	ν_{23}	126	138	125	137	142
E	τ CH_3	ν_{24}	114	112	114	112	112
A_2	τ CH_3	ν_{12}	102	102	103	102	
rmsd (cm^{-1})			73.6	4.0	70.4	4.4	

[a] With the scale factors included in Table 6. [b] With the scale factors included in Table S9.

Spectroscopic Analysis. The 36 vibrational normal modes of ITMG with C_{3v} symmetry (Figure 3) are classified in three symmetry species: $8A_1$ (IR, Ra) + $4A_2$ + 12E (IR, Ra). The A_2 modes are not observed in IR and Raman spectra due to symmetry selection rules. The harmonic frequencies resulting from exploratory calculations are shown in Table S6.

The density functional methods explored all systematically overestimate the higher vibrational frequencies. The inverse situation can be observed for the lower frequencies. These effects are essentially due to the neglect of the anharmonicity of the vibrations in the calculations, especially for CH modes, and the basis set deficiencies, even taking into account the electronic correlation corrections. The hybrid B3LYP method gives somewhat better results than the B3PW91 method.

It is evident from Table S6 that the 6-311G** and LanL2DZdp basis sets present the smallest deviations from the experimental values. The addition of polarized functions clearly improves the quality of the calculated frequencies. Through supplementary functions each valence orbital of the molecule can be represented by a higher number of basis functions, resulting in molecular orbitals that better describe the molecular geometry. The B3LYP/6-311G** combination reproduces the observed frequencies with a root-mean-square deviation (rmsd) of 73.6 cm^{-1}, and the B3LYP/LanL2DZdp gives an rmsd of 70.4 cm^{-1}. The improved performance of the ECP basis sets has already been observed by Jonas et al. when calculating the structure and some properties, such as reaction energies of isodesmic reactions, of the series $(CH_3)_nMCl_{4-n}$ (M = C, Si, Ge, Sn, and Pb; n = 1, 2, 3).[28] It was also observed by Montejo et al. when calculating the harmonic frequencies and the SQM force field of $(CH_3)_3$-SiI.[12]

The frequencies calculated with these methods for $(CH_3)_3$-GeI and the descriptions of their vibrational modes are presented in Table 4 along with the experimental values.

Band Assignment. The observed experimental frequencies agree well with those reported previously.[4] Assignment of the experimental bands to the normal modes of vibration of the molecule was based on the existing vibrational analysis,[4] the results obtained from the theoretical calculations, and the potential-energy distribution (PED). In the following discussion results obtained using the B3LYP/6-311G** method will be referred to. All the observed bands in the vibrational spectra are shown in Table 1 along with their relative intensities, polarization ratios, and the proposed assignments.

Methyl Group Modes. *Stretching Modes.* Only two bands in the CH_3 stretching region, located at 2995 and 2913 cm^{-1}, were previously observed.[4] They were assigned to the antisymmetric and symmetric modes, respectively. However, as a result of the current vibrational analysis, the presence of five bands is expected from the motion of the CH bonds of the three methyl groups present in the molecule. Three belong to the antisymmetric stretches (ν_1, ν_{13}, ν_{14}), and two belong to the symmetric ones (ν_2, ν_{15}).

RTIR spectra (Figure 1) show two groups of bands with several shoulders in this region. The first one is divided into three bands at 2992 cm^{-1}, at 2981 cm^{-1}, and a less intense one at 2975 cm^{-1}. These are attributed to the ν_{13}, ν_1, and ν_{14} antisymmetric stretching modes, respectively. The feature at 2975 cm^{-1} became more intense and better defined when the temperature was decreased and LTIR spectra were recorded (Figure 5). In the Raman spectrum, a depolarized band (2979 cm^{-1}), assigned to the ν_1 mode, appears with a shoulder at 2991 cm^{-1} (Figure 2), which was assigned to the ν_{13} stretching mode. The second group of bands was assigned to the symmetric stretching modes and included a shoulder at 2910 cm^{-1} and a band at 2906 cm^{-1}, attributed to the ν_2 and ν_{15} modes. This shoulder appears well-defined in the LTIR spectra. Only one

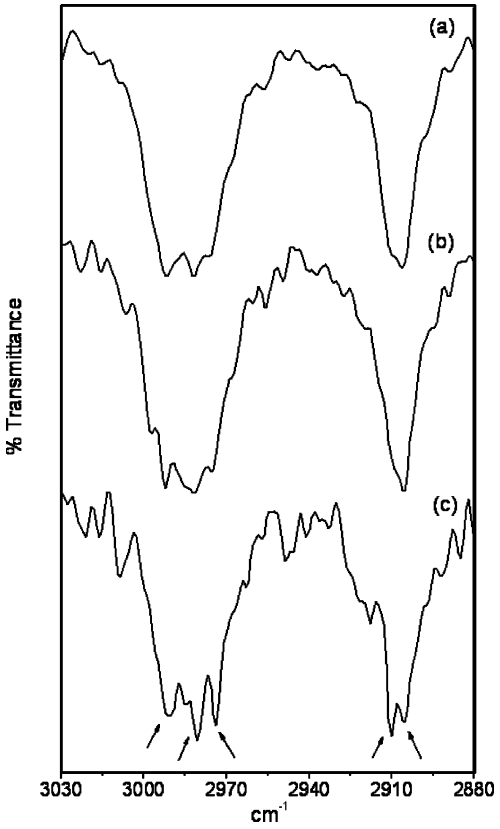

Figure 5. FTIR spectra of the region containing the CH_3 stretching modes at (a) room temperature, (b) −30 °C, and (c) −100 °C.

totally polarized and very intense band was observed in the Raman spectrum, at 2908 cm^{-1}.

The theoretical calculations show important deviations from the experimental frequencies in this region and predict only a very small splitting between the CH_3 stretches. However, the scaled frequencies agree very well with the experimental ones and were useful to estimate the inactive ν_9 (A_2) mode, which lies 2 cm^{-1} below ν_{13}.

Although all bands corresponding to the CH_3 stretching modes could be observed in the RTIR spectrum, the LT spectra improve the resolution of the shoulders, allowing their exact positions to be determined, confirming their assignments to fundamental modes.

Deformation Modes. The three antisymmetric (ν_3, ν_{16}, and ν_{17}) and two symmetric (ν_4 and ν_{18}) CH_3 deformation modes appear in the 1500−1200 cm^{-1} region as described previously.[4] We observed a broad band at 1405 cm^{-1}, assigned to the ν_{16} deformation mode, and a narrow, strong band at 1240 cm^{-1}, which belongs to the ν_4 mode in the RTIR spectrum. In the Raman spectrum the former band appears as a weak absorption at the same frequency while the latter is more intense and appears at 1249 cm^{-1}. Both bands are accompanied by several shoulders. Fourier self-deconvolution (FSD) was applied to this region to determine the remaining bands. The result was the appearance of two bands at 1414 and 1397 cm^{-1} that might correspond to the other two antisymmetric modes (ν_3 and ν_{17}) and one band at 1232 cm^{-1} corresponding to the symmetric vibration ν_{18}. These frequency values are in good accord with the scaled frequencies obtained from the SQM force field.

To confirm this assignment, the RTIR and LTIR spectra were compared. Several shoulders present in the RTIR spectrum were resolved in the LT spectra. As can be seen from Figure 6, the broad band at 1405 cm^{-1} resolves into three bands at 1418,

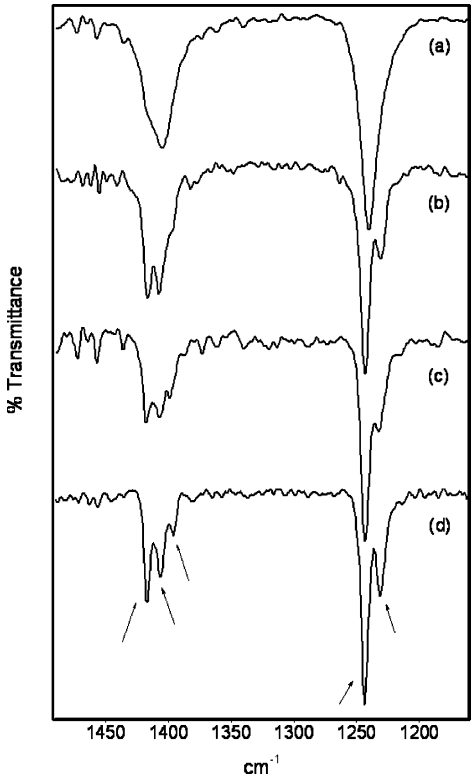

Figure 6. FTIR spectra of the region containing the CH_3 deformation modes at (a) room temperature, (b) −70 °C, (c) −100 °C, and (d) −170 °C.

1407, and 1399 cm^{-1}, which are assigned to the ν_3, ν_{16}, and ν_{17} CH_3 antisymmetric deformation modes, respectively. The other band at 1240 cm^{-1} appears as two bands at 1244 and 1232 cm^{-1}, attributed to the corresponding ν_4 and ν_{18} symmetric deformation modes. Theoretical calculations predict the ν_{10} antisymmetric mode (A_2) to be at 1393 cm^{-1}.

Rocking Modes. A single very strong band at 829 cm^{-1} with shoulders on the high-frequency side was observed in the RTIR spectrum. Its counterpart in the Raman spectrum (833 cm^{-1}) was polarized, confirming its assignment to the totally symmetric ν_5 mode. In the LTIR spectra the ν_5 mode shifts to 826 cm^{-1} and a new band appears at 845 cm^{-1}; this was assigned to the ν_{19} rocking vibration. This band appears by FSD at 843 cm^{-1}, in agreement with the observation from the LT spectra (Figure 7). Previously, only one band was observed in this region, at 840 cm^{-1} in the infrared spectrum of the liquid, which was also assigned to the ν_{19} rocking mode.[4] The feature at 763 cm^{-1} in both the RTIR and LTIR spectra is due to the ν_{20} rocking mode, which appears in the Raman spectrum (760 cm^{-1}) as a very weak depolarized band. This band was observed previously at 765 cm^{-1} in the infrared spectrum of the liquid[4] but, unlike in this work, was not observed in the Raman spectrum. The values of the theoretical frequencies after scaling were used as a guide for the assignment of these bands. Furthermore, the ν_{11} inactive mode was predicted to be at 716 cm^{-1}.

Torsional Modes. A weak depolarized band was found at 112 cm^{-1} in the Raman spectrum, and was assigned to one of the torsional modes of the methyl groups, more specifically to the ν_{24} mode belonging to E symmetry. [The other torsional mode (A_2 symmetry) is inactive in the infrared and Raman spectra.] This band was not observed in earlier work,[4] and the assignment is based on the relative position of the band predicted by the calculations, which should be confirmed by further studies.

GeC_3 Modes and GeI stretching Mode. This group of bands has already been observed previously.[4] The frequency values

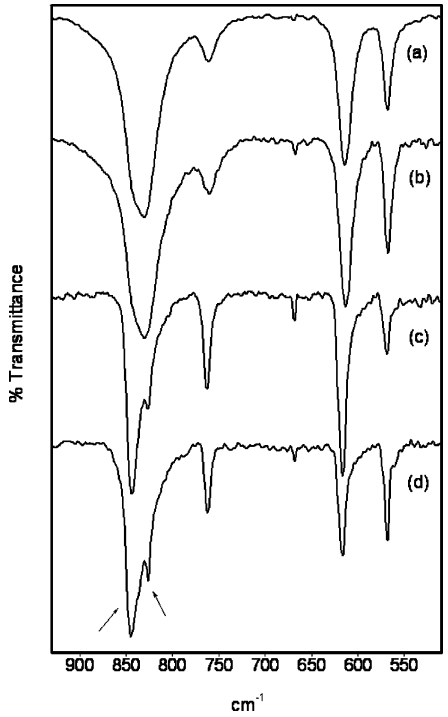

Figure 7. FTIR spectra of the region containing the CH_3 rocking modes at (a) room temperature, (b) −70 °C, (c) −100 °C, and (d) −170 °C.

obtained in this work are in excellent agreement with those previously reported. The measured range is 4000−400 cm^{-1}; therefore, only two of the GeC_3 modes could be observed in the infrared spectra. The profile of these bands remained unchanged when the sample was cooled in liquid nitrogen, as shown in the LTIR spectrum of Figure 7.

The antisymmetric GeC_3 stretching mode (ν_{21}), observed at 614 cm^{-1}, is also observed in the Raman spectrum as a depolarized band with the same frequency. At low temperature it is shifted to 617 cm^{-1}. The corresponding symmetric mode (ν_6), which produces the most intense band, is observed in the Raman spectrum at 569 cm^{-1}. In the RTIR spectra it also appears as a strong band at 568 cm^{-1}.

The GeI stretching mode (ν_7) was observed as a polarized strong band at 220 cm^{-1}. The band at 176 cm^{-1} was assigned to the symmetric GeC_3 ν_8 deformation mode. The ν_{22} antisymmetric deformation mode for GeC_3 had not been observed before. The theoretical calculations predict differences of between 16 and 19 cm^{-1} for the vibrational modes ν_8 and ν_{22} (B3LYP/6-311G**, ν_8 = 183 cm^{-1} and ν_{22} = 167 cm^{-1}; B3LYP/LanL2DZ, ν_8 = 187 cm^{-1} and ν_{22} = 168 cm^{-1}). Careful inspection reveals a shoulder around 190 cm^{-1} in both the parallel and perpendicular Raman spectra. In order to establish the position and relative intensity of the band, the FSD technique, followed by curve-fitting, was used. The approximate frequency value from the FSD was used to calculate the relative intensity of the band by curve-fitting. The resulting frequency value was 189 cm^{-1}, and the relative intensities of the band in the two spectra were used to calculate the polarization ratio, which was 0.65 (Figure 8). This value confirms the assignment of this band to the GeC_3 antisymmetric deformation mode. The GeC_3 (ν_{23}) rocking mode emerges as a medium intensity band at 142 cm^{-1}.

Calculation of Force Constants. The scaling procedure was performed following the method described in the Computational Methods section. The definition of the symmetry coordinates used in the calculation is given in Table S7. The scaled (SQM) force field (Table S8) was also used to calculate the internal force constants which are listed in Table 5.

The harmonic force constants were calculated at the B3LYP level of theory with both the 6-311G** and LanL2DZdp basis sets. The agreement between the calculated and observed vibrational frequencies after scaling the force field was better with the B3LYP/6-311G** method. The force constants presented in the text are therefore those calculated at this level. The resulting rmsd values for the two methods and the scaled frequencies are shown in Table 4. The scale factors, force constants, and PED, which came from the B3LYP/LanL2DZdp calculation, are in Tables S9−S11.

The initial scale factors were taken as unity and were then refined by least-squares fitting to experimental vibrational frequencies. The corresponding calculated frequencies were used for the inactive A_2 modes. The number of scale factors was

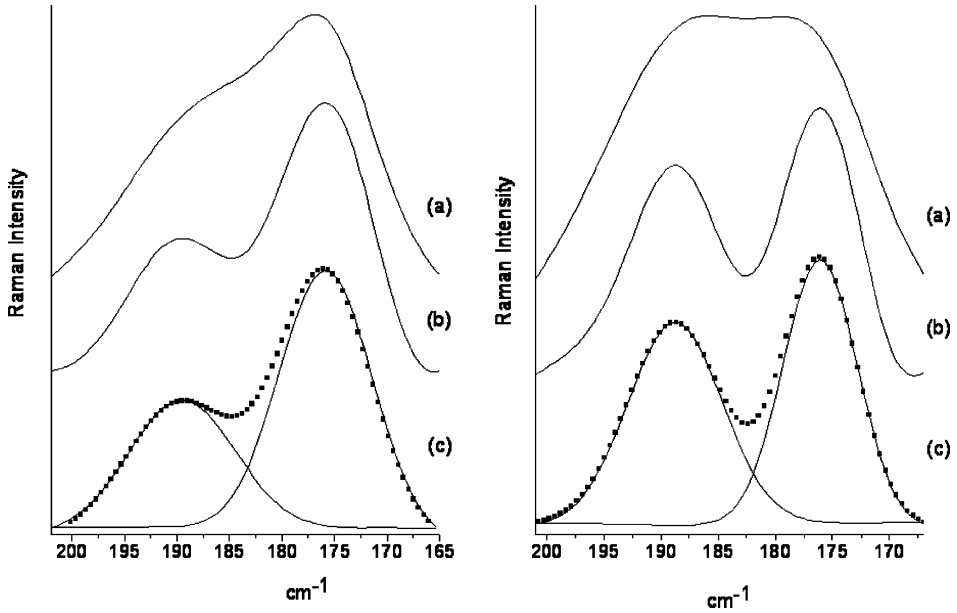

Figure 8. Results of the FSD and curve-fitting for parallel (right) and perpendicular (left) Raman spectra. (a) Original spectrum, (b) Fourier self-deconvolution of the original spectrum (K = 2, W = 20; K = 2, W = 10, respectively) with Gaussians, (c) results of curve-fitting the deconvoluted spectrum with Gaussians (R^2 = 0.9951, χ^2 = 12.60; R^2 = 0.9699, χ^2 = 5.30), respectively.

TABLE 5: Internal Force Constants for ITMG Calculated at the B3LYP/6-311G Level**

	force constant	
coordinate	this work[a]	Anderson[b]
f(CH)	4.82	4.81
f(GeI)	1.31	1.13
f(GeC)	2.71	2.87
f(CGeC)	0.50	0.42
f(CGeI)	0.54	0.48
f(HCH)	0.41	0.50
f(HGeC)	0.34	0.36; 0.50
f(HCGeI)	0.02	
f(CGeC/CGeC)	−0.06	
f(CGeI/CGeI)	−0.08	
f(HCH/HCH)	−0.10	−0.0059
f(HCGe/HCGe)	−0.06	−0.0061; −0.0336

[a] Units are mdyn $Å^{-1}$ for stretching and stretching/stretching interactions and mdyn Å rad^{-2} for deformations and deformation/deformation interactions. [b] Calculated with the SVFF method, taken from ref 4.

TABLE 6: Refined Scale Factors for the Force Field of IMTG Calculated at the B3LYP/6-311G Level**

vibrational mode[a]	scale factor
ν_a CH_3	0.912
ν_s CH_3	0.917
δ_a CH_3	0.921
δ_s CH_3	0.932
ρ CH_3	0.949
ν_a GeC_3, ν_s GeC_3	1.076
ν GeI	0.905
δ_a GeC_3, δ_s GeC_3, ρ GeC_3[b]	1.150
τ CH_3	0.961

[a] ν, stretching; δ, angular deformation; ρ, rocking; τ, torsion; s, symmetric; a, antisymmetric. [b] These modes were not grouped together despite having the same value to be consistent with studies on the related $(CH_3)_3GeX$ (X = H, Cl, and Br).

reduced from 24 to 11 by grouping. The rmsd decreased from an initial value of 73.6 cm^{-1} to 4.0 cm^{-1}, indicating that the scaled frequencies are in excellent agreement with the experimental ones. The scale factors corresponding to each internal force constant for the B3LYP/6-311G** combination are shown in Table 6. The scale factors can be divided into two groups: those where values are <1 as a result of overestimation of the vibrational frequencies and those where values are >1 as a consequence of underestimation of the frequencies.

The SQM force field obtained by this method was employed to calculate the potential-energy distribution (PED), which represents the relative contributions of all the symmetry coordinates to the normal modes of vibration. The PED is given in Table 7 and shows that most of the normal modes are described by more than one symmetry coordinate and, consequently, strong mixing occurs between them. The small number of pure modes involve the motion of the GeC_3 moiety, except for the symmetric deformation (ν_8), which is mixed with the GeI stretching mode (ν_7).

Comparison between $GeIMe_3$ and $SiIMe_3$. In order to compare the valence force constants obtained for ITMG with the corresponding force constants for iodotrimethylsilane, calculations were performed at the same level for both compounds (B3LYP/6-311G**). The experimental frequencies employed for the scaling method and the starting scale factors for the $Si(CH_3)_3$ group were obtained from the literature.[12,29] Scale factors, force constants, and the PED that result from the calculations are given in Tables S12−S14.

Important data are summarized in Table 8, comparing the M−I and M−C (M = Ge, Si) stretching frequencies and the corresponding force constants and bond distances for both compounds. The correlation of vibrational frequencies to the bond strengths and the molecular structure, established by Badger,[30] is of particular interest. From Table 8 it can be seen that the SiI bond is stronger than the GeI bond, as evidenced by the greater stretching frequency and force constant. The SiI and GeI bond distances are in accordance with the vibrational data. A smaller bond distance corresponds to a higher stretching frequency, in good agreement with Badger's rules. The same behavior is shown by the Ge−C and Si−C bonds, and it is in accord with the observed decrease of the dissociation energies of M−C and M−I bonds measured for MX_4 type compounds, when going from the Si to Pb in the periodic table.[31]

To gain insight into the chemical properties of the M−I and M−C bonds, a natural bond orbital (NBO) analysis was performed for both molecules. This analysis is based on a method for optimally transforming a given *N*-electron wave function $\psi = (1, 2, ..., N)$ into wave functions localized in one center and two centers, representing the "lone pair" and the "bond" elements of the Lewis structure picture, respectively. Thus, electron density is constrained to doubly occupied "localized bonding" units. The effect of delocalization appears as weak departures from the idealized localized picture. Hence, the transformation of DFT wave functions to the NBO form is convenient for chemical purposes because the standard valence concepts can be applied to the molecule.

The NBO approach provides the most accurate "natural Lewis structure" picture for describing the electron density $\rho(r)$ of ψ. A simple bond orbital picture is represented by a bonding NBO σ_{AB} which can be written in terms of two natural hybrid orbitals (NHOs), h_A and h_B, on atoms A and B, with corresponding polarization coefficients c_A and c_B, $\sigma_{AB} = c_A h_A + c_B h_B$, termed a Lewis (L) orbital. Each valence bonding NBO is paired with a corresponding valence antibonding NBO (σ^*_{AB}), $\sigma^*_{AB} = c_A h_A - c_B h_B$, termed a non-Lewis (NL) orbital.[32,33] The antibonding orbitals play an important role in departures from the idealized Lewis structure mainly due to their involvement in the delocalization of the electron density. The weakly occupied Rydberg orbitals complete the span of the valence space, but they normally have only a small contribution to the molecular properties. The electronic delocalizations within the L and NL orbitals may be interpreted as charge transfer (CT) between filled (donor) and unfilled (acceptor) orbitals. All of the possible donor−acceptor interactions can be determined from the analysis of the off-diagonal elements in the Fock matrix, calculated by second-order perturbation theory.

In Table 9 the calculated natural hybrids h_A are summarized. These consist of the NBOs along with the polarization coefficient (c_A), the hybrid composition, and the percentages of s, p, and d character of each h_A for each compound. Examination of the results reveals that the p character of the natural orbitals involved in the σ_{GeC} and σ_{GeI} NBOs is higher than the p character for the σ_{SiC} and σ_{SiI}. This is in accord with the lengthening of the GeC and GeI bond distances. Furthermore, a slight mixture of d character occurs in the M−C and M−I bond hybrids, with more mixing in the silicon compound. Also, the iodine atom uses a slightly higher d character in bonding to silicon than to germanium. On the other hand, the carbon NHO of the σ_{CH} bond orbital shows a smaller p character for the germanium than for the silicon compound, evidenced by the shorter CH bond length in $(CH_3)_3GeI$ than in $(CH_3)_3SiI$.

The lengthening of the bond distances is also related to the occupancies of the bonding and antibonding orbitals. Table 10 shows the occupancies of all the natural bond orbitals and the

TABLE 7: Experimental and Calculated Wavenumbers and Assignment of ITMG Calculated at the B3LYP/6-311G Level**

mode	exptl[a]	calcd[a]	SQM[b]	IR intensities[c]	Raman activity[d]	PED[e] (≥10%)	assignment[f]
A_1							
1	2981	3116	2976	17.0	225.5	32% S_1 + 16% S_{15} + 47% S_{16}	ν_a CH_3
2	2910	3037	2908	12.2	467.9	32% S_2 + 16% S_{17} + 46% S_{18}	ν_s CH_3
3	1418	1476	1418	4.8	1.0	31% S_3 + 10% S_{19} + 27% S_{20} + 20% S_{21}	δ_a CH_3
4	1244	1288	1243	<0.1	8.9	34% S_4 + 20% S_{23} + 50% S_{24}	δ_s CH_3
5	826	855	838	143.5	0.8	26% S_5 + 16% S_{27} + 44% S_{28}	ρ CH_3
6	568	549	569	15.6	36.3	100% S_6	ν_s GeC_3
7	220	225	222	31.4	4.4	77% S_7 + 29% S_8	ν GeI + δ_s GeC_3
8	176	162	167	0.4	6.4	63% S_7 + 58% S_8	ν GeI + δ_s GeC_3
A_2							
9		3134	2992	0.0	0.0	34% S_9 + 17% S_{13} + 50% S_{14}	ν_a CH_3
10		1452	1393	0.0	0.0	33% S_{10} + 20% S_{19} + 29% S_{22}	δ_a CH_3
11		736	716	0.0	0.0	37% S_{11} + 37% S_{25} + 12% S_{26} + 15% S_{32}	ρ CH_3 + δ_a GeC_3
12		102	102	0.0	0.0	39% S_{12} + 16% S_{35} + 48% S_{36}	τ CH_3
E							
13	2992	3135	2994	7.3	103.0	34% S_9 + 67% S_{13}	ν_a CH_3
14	2992	3135	2994	7.3	103.0	34% S_9 + 17% S_{13} + 50% S_{14}	ν_a CH_3
15	2974	3115	2973	1.3	39.9	32% S_1 + 63% S_{15}	ν_a CH_3
16	2974	3115	2973	1.3	39.9	32% S_1 + 16% S_{15} + 47% S_{16}	ν_a CH_3
17	2905	3035	2905	6.1	12.5	32% S_2 + 63% S_{17}	ν_s CH_3
18	2905	3035	2905	6.1	12.5	32% S_2 + 16% S_{17} + 47% S_{18}	ν_s CH_3
19	1407	1464	1406	5.9	0.1	31% S_3 + 37% S_{19} + 26% S_{22}	δ_a CH_3
20	1407	1464	1406	5.9	0.1	31% S_3 + 29% S_{20} + 20% S_{21}	δ_a CH_3
21	1399	1460	1403	1.1	17.6	33% S_{10} + 26% S_{20} + 38% S_{21}	δ_a CH_3
22	1399	1460	1403	1.1	17.6	33% S_{10} + 20% S_{19} + 29% S_{22}	δ_a CH_3
23	1232	1276	1233	9.6	1.0	34% S_4 + 70% S_{23}	δ_s CH_3
24	1232	1276	1233	9.6	1.0	34% S_4 + 15% S_{23} + 55% S_{24}	δ_s CH_3
25	845	863	847	36.5	1.1	37% S_{11} + 37% S_{25} + 12% S_{26} + 15% S_{32}	ρ CH_3 + δ_a GeC_3
26	845	863	847	36.5	1.1	37% S_{11} + 49% S_{26} + 20% S_{31}	ρ CH_3 + δ_a GeC_3
27	763	772	754	6.5	0.4	26% S_5 + 60% S_{27}	ρ CH_3
28	763	772	754	6.5	0.4	26% S_5 + 14% S_{27} + 46% S_{28}	ρ CH_3
29	617	595	617	20.9	10.8	97% S_{29}	ν_a GeC_3
30	617	595	617	20.9	10.8	97% S_{30}	ν_a GeC_3
31	189	171	183	2.0	2.9	112% S_{31} + 12% S_{33}	δ_a GeC_3 + ρ GeC_3
32	189	171	183	2.0	2.9	112% S_{32} + 12% S_{34}	δ_a GeC_3 + ρ GeC_3
33	142	126	138	0.4	3.1	106% S_{33}	ρ GeC_3
34	142	126	138	0.4	3.1	106% S_{34}	ρ GeC_3
35	112	114	112	<0.1	<0.1	39% S_{12} + 64% S_{35}	τ CH_3
36	112	114	112	<0.1	<0.1	39% S_{12} + 16% S_{35} + 48% S_{36}	τ CH_3
rmsd (cm^{-1})		73.6	4.0				

[a] Observed and calculated values in cm^{-1}. [b] From scaled quantum mechanics force field (see text). [c] Units: km mol^{-1}. [d] Units: $Å^4$ $(amu)^{-1}$. [e] See Table S7 for definitions of the symmetry coordinates. [f] ν, stretching; δ, angular deformation; ρ, rocking; τ, torsion; s, symmetric; a, antisymmetric.

TABLE 8: Comparison of $(CH_3)_3GeI$ and $(CH_3)_3SiI$

	$(CH_3)_3GeI$		$(CH_3)_3SiI$	
	exptl[a]	calcd[b]	exptl[c]	calcd[b]
ν(MI)	220	225	326	320
f(MI)		1.31		1.64
r(MI)	2.540	2.606	2.485	2.530
ν(MC)	614; 569	595; 549	627	669; 615
f(MC)		2.71		3.00
r(MC)	1.954	1.966	1.870	1.878

[a] Experimental frequencies and bond distances from this work. [b] Theoretical frequencies, force constants, and bond distances calculated using the SQM force field of B3LYP/6-311G**. [c] Experimental frequencies and bond distances from ref 12.

corresponding energies for the germanium and silicon compounds. The increase in σ^* occupancy results in a lengthening of the bond distances. For instance, the σ^*_{GeI} and σ^*_{SiI} occupancies were found to be 0.060 91 and 0.058 51, respectively, with GeI and SiI bond distances of 2.540 and 2.485 Å. The increase in σ^* orbital occupancy results in a weakening of the bond, shown also by the decrease of the vibration frequency (Table 8).

To investigate the nature and magnitude of the intramolecular interactions of Ge and Si compounds, the electron distribution has been analyzed. Table 11 shows the principal delocalizations for the Si and Ge compounds and their associated stabilization energies. For both compounds, the largest contributions to delocalization of the electronic density come from the electron density in the lone pair of the iodine atom [LP(I)] and the σ_{MC} orbital.

From Table 11, the LP(I) → σ^*_{MC} negative hyperconjugation interaction is higher for the silicon compound due to a higher polarization of the acceptor orbital toward the silicon atom, improving its ability as an acceptor. The σ^*_{SiC} polarization toward silicon atom makes a more effective orbital overlap possible as polarization increases the relative strength of interaction. The slight changes in the polarization coefficients of the NHOs are associated with the atomic electronegativity differences (see Table 9). For $(CH_3)_3GeI$, the σ_{GeC} → σ^*_{GeC} and σ_{GeC} → σ^*_{GeI} interactions are also important. Despite the lower polarization of the bonding orbitals toward Ge atom, the low-energy gap between the donor−acceptor orbitals results in a higher value of σ_{GeC} → σ^*_{GeC} and σ_{GeC} → σ^*_{GeI} interactions.

Conclusions

A complete investigation of the molecular structure of ITMG has been carried out in the gas phase by gas electron diffraction complemented by theoretical methods. Both methods agree that $GeIMe_3$ has C_{3v} symmetry, and as for $SiIMe_3$, a pseudopotential

TABLE 9: Calculated Natural Hybrid Orbitals (NHOs) and the Polarization Coefficients (c_A's) of Each Hybrid in the Corresponding NBO for $(CH_3)_3GeI$ and $(CH_3)_3SiI$

type	atom	hybrid composition	% s	% p	% d	c_A	atom	hybrid composition	% s	% p	% d	c_A
σ_{MC}	Ge	$sp^{2.53}d^{0.01}$	28.24	71.53	0.23	0.5706	Si	$sp^{2.55}d^{0.03}$	27.94	71.26	0.79	0.5435
	C	$sp^{2.86}$	25.93	74.03		0.8212	C	$sp^{2.34}$	29.90	70.04		0.8394
σ_{MI}	Ge	$sp^{5.42}d^{0.05}$	15.46	83.80	0.75	0.5673	Si	$sp^{4.97}d^{0.07}$	16.56	82.35	1.09	0.5642
	I	$sp^{7.23}d^{0.03}$	12.10	87.51	0.40	0.8235	I	$sp^{5.72}d^{0.03}$	14.81	84.68	0.51	0.8257
$\sigma_{CH\alpha}$	C	$sp^{3.09}$	24.44	75.49		0.7801	C	$sp^{3.32}$	23.13	76.81		0.7824
	H	S	99.95			0.6256	H	s	99.96			0.6228
$\sigma_{CH\beta}$	C	$sp^{3.03}$	24.77	75.17		0.7830	C	$sp^{3.26}$	23.46	76.48		0.7851
	H	s	99.96			0.6220	H	s	99.96			0.6193

TABLE 10: Calculated σ and σ^* Occupancies with Their Respective Energies for $(CH_3)_3GeI$ and $(CH_3)_3SiI$

	$(CH_3)_3GeI$		$(CH_3)_3SiI$	
orbital type	occupancy	energy (au)	occupancy	energy (au)
σ_{MC}	1.970 97	−0.522 81	1.979 65	−0.530 25
σ^*_{MC}	0.054 72	0.171 33	0.051 16	0.226 71
σ_{MI}	1.966 40	−0.469 25	1.967 82	−0.498 01
σ^*_{MI}	0.060 91	0.027 76	0.058 51	0.055 26
$\sigma_{CH\alpha}$	1.985 54	−0.520 68	1.982 52	−0.513 67
$\sigma^*_{CH\alpha}$	0.004 63	0.400 20	0.005 89	0.394 55
$\sigma_{CH\beta}$	1.990 73	−0.518 83	1.988 27	−0.512 30
$\sigma^*_{CH\beta}$	0.003 13	0.410 62	0.003 72	0.405 90

TABLE 11: Principal Delocalizations for $(CH_3)_3GeI$ and $(CH_3)_3SiI$ with Their Associated Stabilization Energies[a]

$(CH_3)_3GeI$		$(CH_3)_3SiI$	
donor−acceptor	$\Delta E(\sigma\sigma^*)$[b]	donor−acceptor	$\Delta E(\sigma\sigma^*)$
$\sigma_{Ge_1C_2} \rightarrow \sigma^*_{Ge_1C_6}$	13.2	$\sigma_{Si_1C_2} \rightarrow \sigma^*_{Si_1C_6}$	6.7
$\sigma_{Ge_1C_2} \rightarrow \sigma^*_{Ge_1C_{10}}$	13.2	$\sigma_{Si_1C_2} \rightarrow \sigma^*_{Si_1C_{10}}$	6.7
$\sigma_{Ge_1C_2} \rightarrow \sigma^*_{GeI}$	15.1	$\sigma_{Si_1C_2} \rightarrow \sigma^*_{SiI}$	9.6
$\sigma_{Ge_1C_6} \rightarrow \sigma^*_{GeI}$	15.1	$\sigma_{Si_1C_6} \rightarrow \sigma^*_{SiI}$	9.6
$\sigma_{Ge_1C_{10}} \rightarrow \sigma^*_{GeI}$	15.1	$\sigma_{Si_1C_{10}} \rightarrow \sigma^*_{SiI}$	9.6
$LP(2)I \rightarrow \sigma^*_{Ge_1C_6}$	12.6	$LP(2)I \rightarrow \sigma^*_{Si_1C_6}$	13.4
$LP(2)I \rightarrow \sigma^*_{Ge_1C_{10}}$	12.6	$LP(2)I \rightarrow \sigma^*_{Si_1C_{10}}$	13.4
$LP(3)I \rightarrow \sigma^*_{Ge_1C_2}$	16.8	$LP(3)I \rightarrow \sigma^*_{Si_1C_2}$	19.0
$LP(3)I \rightarrow \sigma^*_{Ge_1C_6}$	4.2	$LP(3)I \rightarrow \sigma^*_{Si_1C_6}$	4.7
$LP(3)I \rightarrow \sigma^*_{Ge_1C_{10}}$	4.2	$LP(3)I \rightarrow \sigma^*_{Si_1C_{10}}$	4.7

[a] Calculated at the B3LYP/6-311G** level. [b] Stabilization energies in kJ mol^{-1}.

was required. The SDB-aug-cc-pVTZ basis set and ECP was found to provide the best results when applied to both germanium and iodine atoms. The reinvestigation of both infrared and Raman spectra at low temperature confirmed the previous assignments of the observed bands.[4] Assignments have also been made for bands that could not be observed previously, such as the ν_{14} and ν_2 CH_3 stretching, the ν_3, ν_{17},and ν_{18} CH_3 deformation, and the ν_5 CH_3 rocking modes. The ν_{24} CH_3 torsional mode was observed in the Raman spectrum. Thus more complete vibrational data are now available for this compound. The application of Fourier self-deconvolution in combination with curve-fitting to the analysis of the Raman spectrum resulted in the identification of a band belonging to the ν_{22} GeC_3 antisymmetric deformation mode. The B3LYP method with basis sets supplemented by polarization and/or diffuse functions (e.g., 6-311G** or LanL2DZdp) produced better results in the prediction of the frequencies of vibrational modes. The scaled quantum mechanical method was applied to the B3LYP force field with the 6-311G** split valence basis set, successfully reproducing the vibrational spectra with a set of 11 scale factors and a deviation of 4 cm^{-1}.

Acknowledgment. A.B.A. thanks CIUNT (Consejo de Investigaciones, Universidad Nacional de Tucumán) and CONICET (Consejo Nacional de Investigaciones Científicas y Técnicas, Argentina) for financial support. S.L.M. thanks the Royal Society of Edinburgh for the award of a RSE/BP Personal Research Fellowship and the EPSRC for the award of a grant for electron diffraction research (EP/D057167/1).

Supporting Information Available: Amplitudes of vibration; correlation matrix and coordinates from the GED experiment; experimental and calculated (B3LYP and B3PW91) vibrational frequencies with different basis sets; definition of symmetry coordinates; SQM matrix of symmetry force constants; refined scale factors for force field (B3LYP/LanL2DZdp); internal force constants (B3LYP/LanL2DZdp); experimental and calculated wavenumbers and assignment of ITMG (B3LYP/LanL2DZdp); refined scale factors for force field of iodotrimethylsilane (ITMS) (B3LYP/6-311G**); internal force constants for ITMS (B3LYP/6-311G**); experimental and calculated wavenumbers and assignment of ITMS (B3LYP/6-311G**), low-level ab initio calculations; weighting points for off-diagonal weight matrices, correlation parameters, scale factors for both camera distances for GED. This material is available free of charge via the Internet at http://pubs.acs.org.

References and Notes

(1) West, R.; Hunt, H. R., Jr.; Whipple, R. O. *J. Am. Chem. Soc*. **1954**, *76*, 310.
(2) Zablotna, R.; Akerman, K.; Szuchnik, A. *Bull. Acad. Pol. Sci., Ser. Sci. Chim.* **1964**, *12*, 695.
(3) U.S. Patent 4,356,327, 1982.
(4) Anderson, J. W.; Barker, G. K.; Drake, J. E.; Hemmings, R. T. *Can. J. Chem*. **1971**, *49*, 2931.
(5) *Spectrum*, Version 5.3; Perkin-Elmer, Inc.: Waltham, MA, 2005.
(6) Kauppinen, J. K.; Moffatt, D. J.; Mantsh, H. H.; Cameron, D. G. *Appl. Spectrosc.* **1981**, *35*, 271.
(7) Kauppinen, J. K.; Moffatt, D. J.; Cameron, D. G.; Mantsh, H. H. *Appl. Opt.* **1981**, *20*, 1866.
(8) Kauppinen, J. K.; Moffatt, D. J.; Holberg, M. R.; Mantsh, H. H. *Appl. Spectrosc.* **1991**, *45*, 411.
(9) Griffiths, P. R.; Pierce, J. A.; Hongjin, G. In *Computer-Enhanced Analytical Spectroscopy*; Meuzelaar, H. L. C., Isenhour, T. L., Eds.; Plenum Press: New York, 1989; Chapter 2.
(10) Friesen, W. I.; Michaelian, K. H. *Appl. Spectrosc.* **1991**, *45*, 50.
(11) Michaelian, K. H.; Friesen, W. I.; Yariv, S.; Nasser, A. *Can. J. Chem.* **1991**, *69*, 1786.
(12) Montejo, M.; Hinchley, S. L.; Ben Altabef, A.; Robertson, H. E.; Ureña, F. P.; Rankin, D. W. H.; López-Gónzalez, J. J. *Phys. Chem. Chem. Phys.* **2006**, *8*, 1.
(13) Frisch, M. J.; Trucks, G. W.; Schlegel, H. B.; Scuseria, G. E.; Robb, M. A.; Cheeseman, J. R.; Montgomery, J. A., Jr.; Vreven, T.; Kudin, K. N.; Burant, J. C.; Millam, J. M.; Iyengar, S. S.; Tomasi, J.; Barone, V.; Mennucci, B.; Cossi, M.; Scalmani, G.; Rega, N.; Petersson, G. A.; Nakatsuji, H.; Hada, M.; Ehara, M.; Toyota, K.; Fukuda, R.; Hasegawa, J.; Ishida, M.; Nakajima, T.; Honda, Y.; Kitao, O.; Nakai, H.; Klene, M.; Li, X.; Knox, J. E.; Hratchian, H. P.; Cross, J. B.; Adamo, C.; Jaramillo, J.; Gomperts, R.; Stratmann, R. E.; Yazyev, O.; Austin, A. J.; Cammi, R.; Pomelli, C.; Ochterski, J. W.; Ayala, P. Y.; Morokuma, K.; Voth, G. A.; Salvador, P.; Dannenberg, J. J.; Zakrzewski, V. G.; Dapprich, S.; Daniels, A. D.; Strain, M. C.; Farkas, O.; Malick, D. K.; Rabuck, A. D.; Raghavachari, K.; Foresman, J. B.; Ortiz, J. V.; Cui, Q.; Baboul, A. G.; Clifford, S.; Cioslowski, J.; Stefanov, B. B.; Liu, G.; Liashenko, A.; Piskorz, P.; Komaromi, I.; Martin, R. L.; Fox, D. J.; Keith, T.; Al-Laham, M. A.; Peng, C. Y.; Nanayakkara, A.; Challacombe, M.; Gill, P. M. W.; Johnson, B.; Chen, W.; Wong, M. W.; Gonzalez, C.; Pople, J. A. *Gaussian 03*, revision B.01; Gaussian, Inc.: Pittsburgh, PA, 2003.

(14) Pulay, P.; Fogarasi, G.; Pongor, G.; Boggs, J. E.; Vargha, A. *J. Am. Chem. Soc.* **1983**, *105*, 7037.
(15) Rauhut, G.; Pulay, P. *J. Phys. Chem.* **1995**, *99*, 3093.
(16) Rauhut, G.; Pulay, P. *J. Phys. Chem.* **1995**, *99*, 14572.
(17) Collier, W. B. *Program FCARTP*; QCPE No. 631; Department of Chemistry, Oral Roberts University: Tulsa, OK, 1992.
(18) Glendening, E. D.; Reed, A. E.; Carpenter, J. E.; Weinhold, F. *NBO*, version 3.1; 1998.
(19) Huntley, C. M.; Laurenson, G. S.; Rankin, D. W. H. *J. Chem. Soc., Dalton Trans.* **1980**, 954.
(20) Fleischer, H.; Wann, D. A.; Hinchley, S. L.; Borisenko, K. B.; Lewis, J. R.; Mawhorter, R. J.; Robertson, H. E.; Rankin, D. W. H. *Dalton Trans.* **2005**, 3221.
(21) Hinchley, S. L.; Robertson, H. E.; Borisenko, K. B.; Turner, A. R.; Johnston, B. F.; Rankin, D. W. H.; Ahmadian, M.; Jones, J. N.; Cowley, A. H. *Dalton Trans.* **2004**, 2469.
(22) Ross, A. W.; Fink, M.; Hilderbrandt, R. *International Tables for Crystallography*; Wilson, A. J. C., Ed.; Kluwer Academic Publishers: Dordrecht, Boston, and London, 1992; Vol. C, p 245.
(23) Sipachev, V. A. *J. Mol. Struct. (THEOCHEM)* **1985**, *121*, 143.
(24) Brain, P. T.; Morrison, C. A.; Parsons, S.; Rankin, D. W. H. *J. Chem. Soc., Dalton Trans.* **1996**, 4589. Blake, A. J.; Brain, P. T.; McNab, H.; Miller, J.; Morrison, C. A.; Parsons, S.; Rankin, D. W. H.; Robertson, H. E.; Smart, B. A. *J. Phys. Chem.* **1996**, *100*, 12280. Mitzel, N. W.; Rankin, D. W. H. *Dalton Trans.* **2003**, 3650.
(25) Martin, J. M. L.; Sundermann, A. *J. Chem. Phys.* **2001**, *114*, 3408.
(26) Aarset, K.; Page, E. M. *J. Phys. Chem. A* **2004**, *108*, 5474.
(27) Chadha, R. K.; Drake, J. E.; Neo, M. K. H. *J. Crystallogr. Spectrosc. Res.* **1985**, *15*, 39.
(28) Jonas, V.; Frenking, G.; Reetz, M. T. *J. Comput. Chem.* **1992**, *13*, 935.
(29) Montejo, M.; Ureña, F. P.; Márquez, F.; López-Gónzalez, J. J. *Spectrochim. Acta* **2005**, *A62*, 1058.
(30) Badger, R. M. *J. Chem. Phys.* **1934**, *2*, 128.
(31) Shaw, C. F.; Allred, A. L. *Organomet. Chem. Rev.* **1970**, *5*, 96.
(32) Curtiss, L. A.; Weinhold, F. *Chem. Rev.* **1988**, *88*, 899.
(33) Weinhold, F.; Landis, C. R. *Chem. Educ. Res. Pract. Eur.* **2001**, *2*, 91.